C. T.-C. Nguyen, "Micromechanical resonators for oscillators and filters," *Proceedings* of the 1995 IEEE International Ultrasonics Symposium, Seattle, WA, pp. 489-499, Nov. 7-10, 1995.

Micromechanical Resonators for Oscillators and Filters

Clark T.-C. Nguyen

Center for Integrated Sensors and Circuits
Department of Electrical Engineering and Computer Science
University of Michigan
Ann Arbor, MI 48109-2122

***Abstract*—Fully monolithic, high-*Q*, micromechanical signal processors are described. A completely monolithic high-*Q* oscillator, fabricated via a combined CMOS plus surface micromachining technology, is detailed, for which the oscillation frequency is controlled by a polysilicon micromechanical resonator to achieve high stability. The operation and performance of μmechanical resonators are modelled, with emphasis on circuit and noise modelling. Micromechanical filter design is described, and a prototype two-resonator bandpass filter is demonstrated. An integrated micro-oven that stabilizes the resonance frequency against temperature variations using only 2 mW of power is reviewed. Brownian motion and mass loading phenomena are shown to have a greater influence on short-term stability and dynamic range in this micro-scale. Scaling strategies are proposed to alleviate potential limitations due to Brownian noise.**

INTRODUCTION

Mechanical tank components are widely used in communication circuits for high-*Q* filtering at the IF and RF frequencies and to generate precision local oscillators. Among the most commonly used mechanical devices are quartz crystals and SAW filters, which are off-chip components that interface with signal processing circuitry at the board level. The current trend to include increasing amounts of a total system on a single silicon chip makes fully monolithic high-*Q* filters and oscillators, where the mechanical element is fabricated on-chip, desirable.

The rapid growth of micromachining technologies, which yield high-*Q* on-chip μmechanical resonators, may now make such systems possible. With *Q*'s of over 80,000 [1] under vacuum and center frequency temperature coefficients in the range of -10 ppm/°C (several times less with nulling techniques) [2], polysilicon micromechanical resonators can serve well as miniaturized substitutes for crystals in a variety of high-*Q* oscillator and filtering applications.

Such an oscillator has recently been demonstrated [3,4], which utilizes a surface-micromachined, polycrystalline silicon resonator [10] frequency-setting element and CMOS electronics to sustain oscillation, all fabricated onto a single silicon chip using a technology that merges CMOS and surface micromachining. In addition, passive μmechanical filters, without on-chip electronics, have also been demonstrated [5,19,20].

This paper reviews the design and performance of micromechanical resonators and presents several specific examples of their application to communication electronics. Discussions for each application will focus upon analysis of the potential impact that miniaturization of high-*Q* tank elements has on overall system performance. For each potential limitation, counteracting design strategies are proposed.

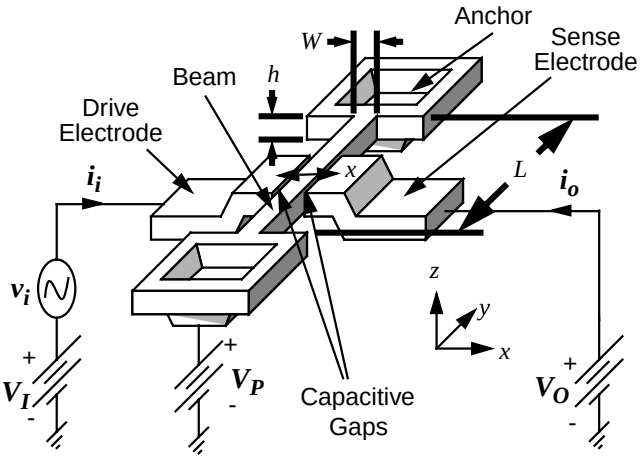

Fig. 1: Perspective view of a two-port parallel-plate capacitively transduced μresonator under a general bias and excitation scheme.

MICROMECHANICAL RESONATORS

To simplify the task of integrating CMOS with micromechanics, capacitive excitation and detection is utilized for the μresonators in this work. A variety of capacitive transducer topologies are available in this technology. The choice of topology dictates the frequency tuning range and stability of the μresonator.

Figure 1 shows the perspective view of a two-port clamped-clamped beam, parallel-plate capacitively transduced μresonator in a typical bias and excitation configuration [7,8]. An infinite number of resonance modes are possible for the structure of Fig. 1 [9]. The frequency of each mode is determined largely by structural material properties and by geometry. For the case of zero axial stress, the resonance frequency f_{rn} of a given mode n for the clamped-clamped beam in the direction indicated (parallel to the substrate) is given by the expression [9]:

$$f_{rn} = \frac{1}{2\pi}\sqrt{\frac{k}{m}} = \frac{K_n}{2\pi}\sqrt{\frac{E}{\rho}}\left(\frac{W}{L^2}\right), \qquad (1)$$

where m is the effective mass of the resonator evaluated at the point of transduction, k is the system spring constant, E is the Young's modulus of the resonator material, ρ is its density, and the geometric quantities L and W are given in Fig. 1. Different modes are distinguished by the constant K_n, which is tabulated for the first five modes in Table 1.

As shown, the complete μresonator device is composed of the clamped-clamped beam resonator, a ground plane underneath and in electrical contract with the beam, and two (or more) capacitive

.

Table 1: Mode Characteristics of Clamped-Clamped Beams

Mode	n	Nodal Points	K_n	f_{rn}/f_o
Fundamental (f_o)	1	2	1.028	1.000
1st Harmonic (f_{r2})	2	3	2.833	2.757
2nd Harmonic (f_{r3})	3	4	5.552	5.404
3rd Harmonic (f_{r4})	4	5	9.182	8.932
4th Harmonic (f_{r5})	5	6	13.717	13.344

transducer electrodes. To bias and excite the device, a dc-bias voltage V_P is applied to the resonator and its underlying ground plane, while an ac excitation voltage is applied to one (or more) drive electrodes. A specific resonance mode may be emphasized by using multiple drive electrodes, placing them at the displacement maxima of the desired mode, and applying properly phased drive signals to the electrodes. To avoid unnecessary notational complexity, however, we focus on the case of fundamental-mode resonance in the present discussion. We also assume that the electrodes are concentrated at the center of the beam and that the beam length is much greater than the electrode lengths. This allows us to neglect beam displacement variations across the lengths of the electrodes due to the beam's mode shape (i.e., we may assume that $x(y) \sim x$ for y near the center of the beam). A more rigorous analysis which accounts for all of these effects is certainly possible, but obscures the main points.

When an ac excitation with frequency close to the fundamental resonance frequency of the μresonator is applied, the μresonator begins to oscillate, creating a time-varying capacitance between the μresonator and the electrodes. Since the dc-bias $V_{Pn} = V_P - V_n$ is effectively applied across the time-varying capacitance at port n, a motional output current arises at port n, given by

$$i_n = -V_{Pn}\frac{\partial C_n}{\partial t} = -V_{Pn}\frac{\partial C_n}{\partial x}\frac{\partial x}{\partial t}, \qquad (2)$$

where x is the displacement at the beam's center (defined in Fig. 1) and $\partial C_n/\partial x$ is the change in capacitance per unit displacement at port n. For a given positive displacement x, the electrode-to-resonator capacitors on the left-hand-side (LHS) decrease, while those on the right-hand-side (RHS) increase. Approximate expressions (neglecting fringing electric fields) for $\partial C_n/\partial x$ may be written as follows:

$$\frac{\partial C_n}{\partial x} = \begin{cases} -\frac{C_{on}}{d_n}\left(1+\frac{x}{d_n}\right)^{-2}, & \text{LHS} \\ \frac{C_{on}}{d_n}\left(1-\frac{x}{d_n}\right)^{-2}, & \text{RHS} \end{cases} \qquad (3)$$

where C_{on} is the static beam-to-electrode capacitance at port n, and d_n is the static electrode-to-resonator gap distance. Note that $\partial C_n/\partial x$ is inversely proportional to the gap distance. As will be shown, the value of $\partial C_n/\partial x$ should be large to suppress μresonator noise and to insure adequate designability of high frequency oscillators and micromechanical filters.

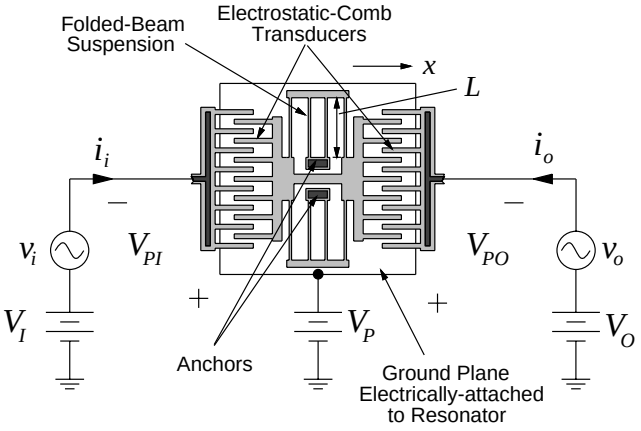

Fig. 2: Overhead view of a two-port, folded-beam, lateral comb-driven resonator with typical applied bias and excitation voltages. All areas of the resonator and electrodes are suspended 2 μm above the substrate, except for the darkly shaded areas, which are the anchor points.

As seen in Eq. (3), the overlap capacitance C_n at port n is nonlinearly dependent upon displacement x, and thus, the change in capacitance vs. displacement $\partial C_n/\partial x$ is a strong function of displacement. This nonlinear dependence leads to not only a nonlinear transfer function, but also to a dependence of the resonance frequency on the dc-bias voltage V_P [19]. To reduce nonlinearity and eliminate this component of frequency instability, the electrode-to-resonator capacitance must be made to vary linearly with resonator displacement. In this work, this is achieved by using interdigitated-comb finger drive and sense capacitors [10].

Figure 2 shows the overhead view of a μresonator which utilizes interdigitated-comb finger transduction in a typical bias and excitation configuration. The μresonator consists of a finger-supporting shuttle mass suspended 2 μm above the substrate by folded flexures, which are anchored to the substrate at two central points. The shuttle mass is free to move in the direction indicated, parallel to the plane of the silicon substrate. Folding the suspending beams as shown provides two main advantages: first, post-fabrication residual stress is relieved if all beams expand or contract by the same amount; and second, spring stiffening nonlinearity in the suspension is reduced [13], since the folding truss is free to move in a direction perpendicular to the resonator motion. A scanning-electron micrograph of a100 kHz version of this μresonator is presented in Fig. 3.

The fundamental resonance frequency of this mechanical resonator is, again, determined largely by material properties and by geometry, and is given by the expression [10,11]:

$$f_o = \frac{1}{2\pi}\left[\frac{2Eh(W/L)^3}{\left(M_P + \frac{1}{4}M_t + \frac{12}{35}M_b\right)}\right]^{1/2}, \qquad (4)$$

where M_P is the shuttle mass, M_t is the mass of the folding trusses, M_b is the total mass of the suspending beams, W and h are the cross-sectional width and thickness, respectively, of the suspending beams, and L is indicated in Fig. 2.

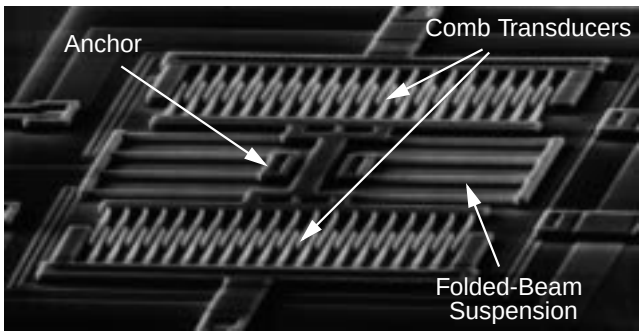

Fig. 3: SEM of a 100 kHz folded-beam, capacitive-comb transduced μresonator.

For this resonator design, the transducer capacitors consist of overlap capacitance between the interdigitated shuttle and electrode fingers. As the shuttle moves, these capacitors vary linearly with displacement. Thus, $\partial C_n/\partial x$ is a constant, given approximately by the expression

$$\frac{\partial C_n}{\partial x} \approx \begin{cases} -\dfrac{\alpha N_g \varepsilon_o h}{d}, & \text{LHS} \\ \dfrac{\alpha N_g \varepsilon_o h}{d}, & \text{RHS} \end{cases} \tag{5}$$

where N_g is the number of finger gaps, h is the film thickness, and d is the gap between electrode and resonator fingers. α is a constant that models additional capacitance due to fringing electric fields. For comb geometries, α=1.2 [12]. Note from (5) that, again, $\partial C_n/\partial x$ is inversely proportional to the gap distance.

Small-Signal Equivalent Circuit.

The equivalent circuit for the two-port resonators of Figs. 1 or 2 can be derived via impedance analyses, and is presented in Fig. 4, along with equations for the respective circuit elements. Typical circuit element values for the case of a 100 kHz, 2 μm-thick comb-transduced resonator with 2 μm electrode-to-resonator gap spacings are also indicated in the figure, as is the simplifying transformation to a series LCR tank when the transducers are identical (i.e., $\partial C_1/\partial x = \partial C_2/\partial x$). For present purposes, the series resistance is of most interest, and is repeated here for convenience:

$$R_{xn} = \frac{\sqrt{km}}{Q\eta_n} \quad \text{, where } \eta_n = V_{Pn}\left(\frac{\partial C}{\partial x}\right)_n, \tag{6}$$

where variables are defined in the caption of Fig. 4.

The equivalent circuit for capacitively transduced resonators with more than two ports is a simple extension of Fig. 4 [1,19].

Quality Factor.

In order to attain high Q, μmechanical resonators should be operated in vacuum to eliminate losses due to fluidic damping mechanisms [14,15,16]. For μmechanical resonators with Q's in the range of 50,000 to 500,000, viscous gas damping ceases to be the dominant energy dissipation mechanism at pressures in the range of 0.1 to 1 mTorr [15], where intrinsic material damping

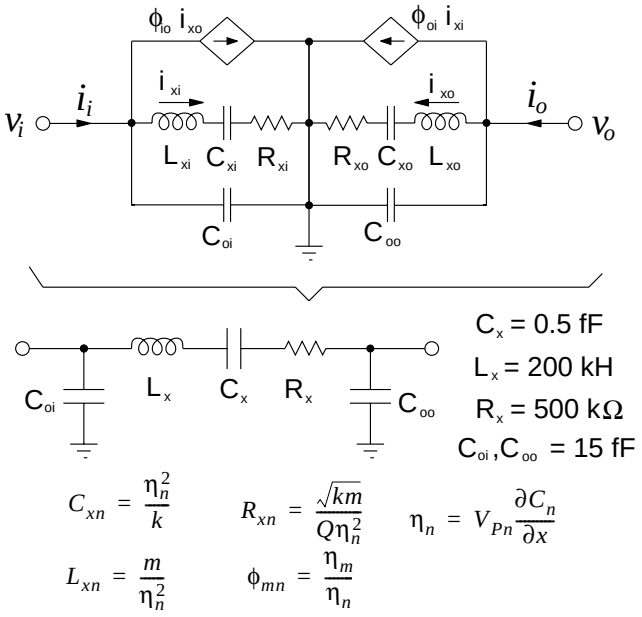

Fig. 4: Equivalent circuit for a two-port μmechanical resonator showing the transformation to the convenient LCR form. In the equations, m is the effective mass of the resonator evaluated at the point of transduction, k is the system spring constant, Q is the quality factor, and $\partial C_n/\partial x$ is the change in capacitance per displacement at port n.

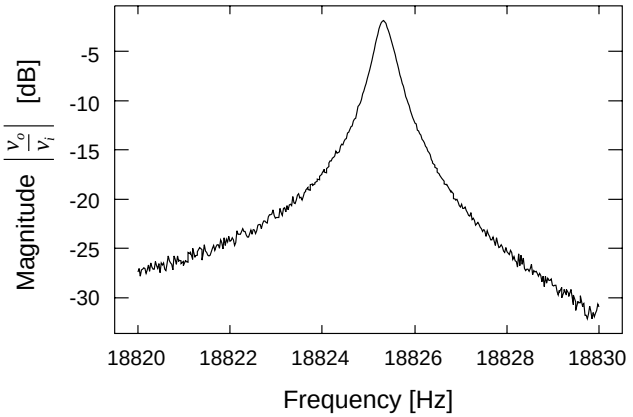

Fig. 5: Measured transconductance spectrum for a folded-beam, capacitive-comb transduced polysilicon μmechanical resonator operated under a vacuum pressure of 20 mTorr.

mechanisms become dominant [17,18], and the Q of the μresonator is maximized with respect to viscous damping.

Figure 5 presents the measured transconductance spectrum for a folded-beam, capacitive-comb transduced polysilicon μmechanical resonator operated under a vacuum pressure of 20 mTorr. The spectrum in Fig. 5 is highly selective, with a quality factor Q of 51,000. For lower pressures, the Q is even larger, exceeding 80,000. This demonstrated degree of frequency selectivity makes μmechanical resonators well suited to high-Q oscillator applications.

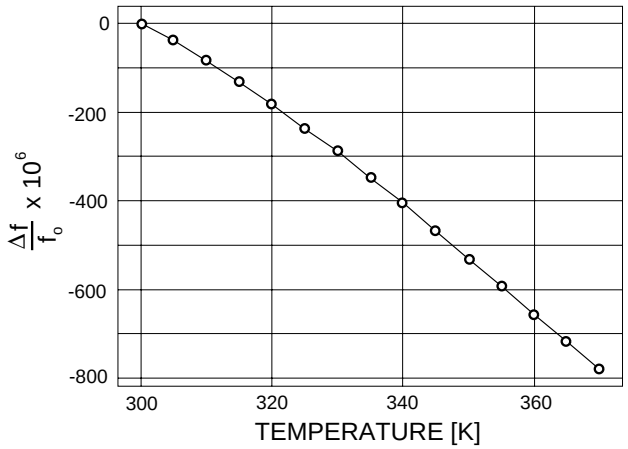

Fig. 6: Measured plot of fractional frequency change $\Delta f/f$ in parts per million vs. temperature for a folded-beam, capacitive-comb transduced polysilicon μmechanical resonator.

Thermal Stability.

The use of a tank element with large quality factor helps to insure excellent short-term frequency stability in oscillators. To insure exceptional long-term stability, the temperature coefficient of the resonance frequency and the aging rate of the tank element must be minuscule.

Figure 6 shows a measured plot of fractional frequency change $\Delta f/f$ versus temperature for a folded-beam, capacitive-comb transduced polysilicon μmechanical resonator. From the slope of the curve, the temperature coefficient of the resonance frequency, TC_{fr}, for this device is –10 ppm/°C. Through manipulation of Eq. (4), the temperature coefficient of the Young's modulus, TC_E, may be expressed as

$$TC_E = 2TC_{fr} - TC_h. \tag{7}$$

Using the measured value of TC_{fr} = –10 ppm/°C, (7) yields TC_E = –22.5 ppm/°C. This value is considerably smaller than a previously reported number [21], and it is stated tentatively pending a more systematic study of other factors which can affect the TC_{fr}.

As will be shown, the measured TC_{fr} of –10 ppm/°C can be reduced via on-chip compensation or on-chip oven control techniques.

Thermal Noise.

If the ambient temperature around a damped mechanical resonator is finite (i.e., not 0 Kelvin), and if the system is in thermal equilibrium, then the mechanical resonator must exhibit some degree of random (Brownian) motion. This random vibration constitutes thermal noise in the mechanical domain.

The magnitude of the random vibration is dependent upon the amount of damping in the oscillator system. To see this, consider that to avoid violating the Second Law of Thermodynamics, the model for a *damped*, simple harmonic oscillator must include a noise force generator with sufficient amplitude to maintain the degree of random vibration dictated by the temperature of the system. Without this noise force generator, the damping of the system would force any oscillation to decay to zero, implying a system temperature of 0 K, which will violate thermal equilibrium requirements if the ambient temperature is not 0 K. Thus, the magnitude of the noise force generator should depend upon both temperature and the amount of damping in the system.

An expression for the noise force f_n can be obtained using the Equipartition Theorem [22,23,19], which states that any mode of a system in thermal equilibrium has an average noise energy of $(1/2)k_BT$, where k_B is Boltzmann's constant (1.38×10^{-23} J/K) and T is the temperature in Kelvin. Through equilibrium arguments [23], the action of all modes (including molecular vibrations, velocity, etc...) may be combined into the action of an "ordered" mode, such as vibration of a mass-spring system. The average noise displacement of the mass in a mass-spring-damper oscillator system, assuming a dominant mode in the x-direction, is given by

$$\frac{1}{2}k\langle x_n^2\rangle = \frac{1}{2}k_BT, \tag{8}$$

where x_n is the displacement noise, and $\langle x_n^2\rangle$ is equal to the integral of $|x_n|^2$ over all frequencies. Inserting the expression for $|x_n|^2$ [19], then integrating and rearranging, the expression for noise force is found to be [23]:

$$\frac{\overline{f_n^2}}{\Delta f} = \frac{4kk_BT}{\omega_o Q} = \frac{4\sqrt{km}k_BT}{Q}. \tag{9}$$

Note that this noise force is white over the thermal bandwidth. In converting from force to displacement, the noise is shaped by the force-to-displacement transfer function of the mechanical resonator. Thus, the displacement noise $\overline{x_n^2}$ peaks at the resonance frequency (where oscillators and μmechanical filters operate). Note that this noise is Q times larger than that for mechanical devices operating below resonance, such as accelerometers [24]. From (9), an expression for noise displacement at resonance may be obtained as follows:

$$\frac{\overline{x_n^2}}{\Delta f} = \frac{Q^2}{k^2}\frac{\overline{f_n^2}}{\Delta f} = \frac{4Q\sqrt{m}k_BT}{k^{3/2}} \tag{10}$$

Using Eq. (10) and the expression for output current as a function of displacement for a capacitively transduced resonator (Eq. (2)), the noise current at resonance is given by

$$\frac{\overline{i_n^2}}{\Delta f} = \omega_o^2 V_P^2\left(\frac{\partial C}{\partial x}\right)^2\frac{\overline{x_n^2}}{\Delta f} = \frac{4k_BT}{R_x} \tag{11}$$

where R_x is the series motional resistance of the microresonator seen at resonance at the port in question. Note that Eq. (11) is exactly the expression for thermal noise in a resistor with value R_x. Off resonance, this noise is shaped by the resonator frequency characteristic. Thus, the thermal noise performance of a micromechanical resonator is modelled completely by the noise performance of its equivalent circuit. For a port-symmetric resonator (i.e., $\eta_1 = \eta_2$), one need only add a noise generator corresponding to the resistor R_x in the equivalent LCR circuit. To minimize thermal voltage noise power in μresonators, this theory suggests that the series resistance R_x be minimized. From (6), this in turn

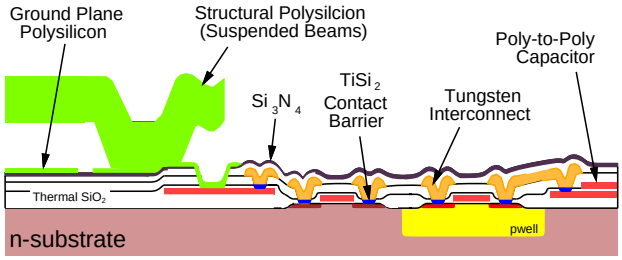

Fig. 7: Cross-section of the MICS technology for integration of CMOS and microstructures.

requires that the electromechanical coupling factor η be maximized. η is largest when V_P and $\partial C/\partial x$ are maximized. Since $\partial C/\partial x$ is maximized when the electrode-to-resonator gaps are minimized, μresonator noise performance improves as the electrode-to-resonator gap decreases.

FABRICATION

To fabricate the described μmechanical resonators, either surface or bulk micromachining technologies may be utilized. For the communications applications to be described, the preferred micromachining technology is often ultimately determined by the ease with which integration with electronics can be achieved, by the properties of the structural material, and by the achievable degree of micromechanical complexity. For example, for some applications surface micromachining may achieve two levels of suspension more easily. On the other hand, μresonators constructed from bulk-micromachined single-crystal silicon may exhibit superior material properties.

To maximize complexity and flexibility, the technology used to fabricate the fully monolithic high-*Q* oscillator to be discussed combines planar CMOS processing with surface micromachining [3,4,5,32]. The technologies are combined in a modular fashion, in which the CMOS processing and surface micromachining are done in separate process modules, with no intermixing of CMOS or micromachining steps. This **M**odular **I**ntegration of **C**MOS and micro**S**tructures (MICS) process has the advantage in that it allows the use of nearly any CMOS process with a variety of surface micromachining processes. A cross-section of the MICS technology is shown in Fig. 7.

In order to avoid problems with microstructure topography, which commonly includes step heights of 2 to 3 μm, the CMOS module is fabricated before the microstructure module. Although this solves topography problems, it introduces constraints on the CMOS. Specifically, the metallization and contacts for the electronics must be able to survive post-CMOS micromachining processing with temperatures up to 835°C. Aluminum interconnect, the industry standard, cannot survive these temperatures. For this reason, tungsten with $TiSi_2$ contact barriers is used as interconnect for this process.

MICROMECHANICAL RESONATOR OSCILLATORS

Figure 8 shows a system-level schematic describing the basic architecture used for this oscillator. Since the motional resistance of the μresonator is large (Fig. 4), a series resonant oscillator architecture is utilized to minimize *Q*-loading [25]. As shown, the system consists of a three-port micromechanical resonator, for

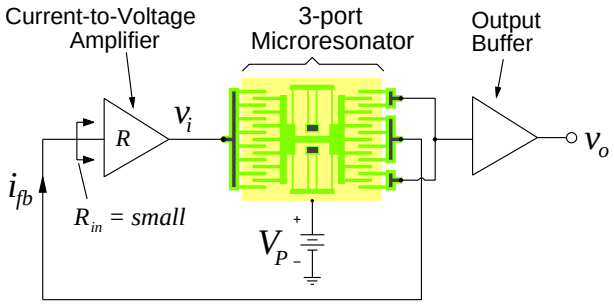

Fig. 8: System level schematic for the μresonator oscillator.

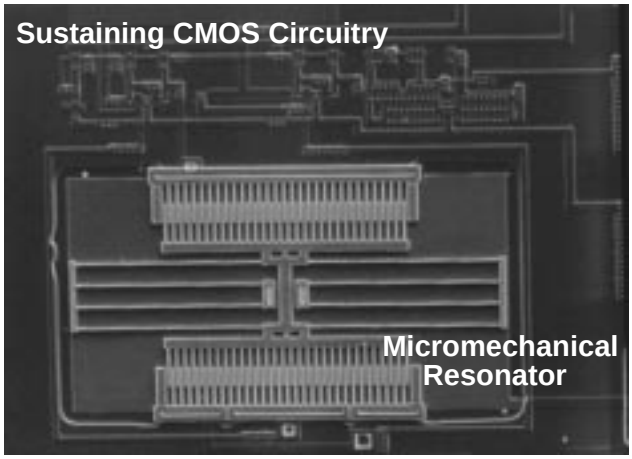

Fig. 9: SEM of a fully monolithic high-*Q* CMOS micromechanical resonator oscillator.

which two ports are embedded in a positive feedback loop with a sustaining transresistance amplifier, while a third port is directed to an output buffer. The use of a third port effectively isolates the sustaining feedback loop from variations in output loading. Conceptually, the sustaining amplifier and μmechanical resonator comprise negative and positive resistances, respectively. (The input and output resistances of the sustaining amplifier also contribute to the total positive resistance, but will be neglected for now.) During start-up, the negative (trans)resistance of the amplifier *R* is larger in magnitude than the positive resistance of the resonator R_x, and oscillation results. Oscillation builds up until either some form of nonlinearity or a designed automatic-level control circuit alters either or both resistors so that, $R=R_x$, at which point the oscillation amplitude limits.

A specific transresistance sustaining amplifier design has been detailed previously in [3], along with methods for voltage control of the oscillation amplitude. Figure 9 presents the SEM of a fully monolithic high-*Q* oscillator fabricated using the CMOS+μStructures process shown in Fig. 7. The complete oscillator, comprised of the aforementioned sustaining amplifier integrated with a 16.5 kHz μmechanical resonator, requires only 500 x 500 μm^2 of area. Higher frequency oscillators that utilize much smaller μresonators require even less area. Figure 10 shows the output waveform of this oscillator measured on an oscilloscope.

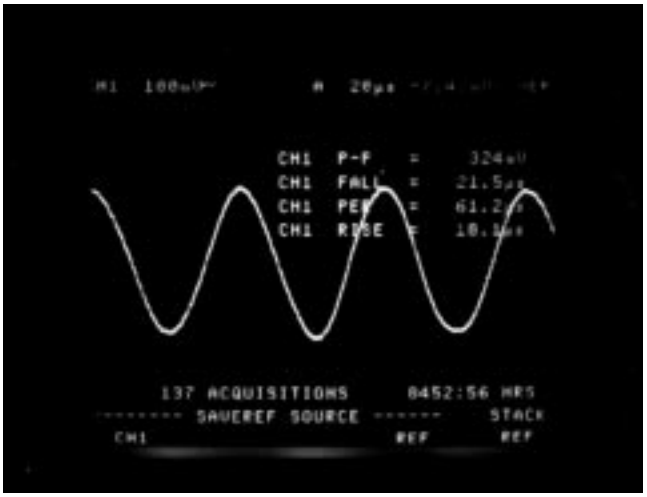

Fig. 10: Oscilloscope waveform for the µresonator oscillator of Fig. 9.

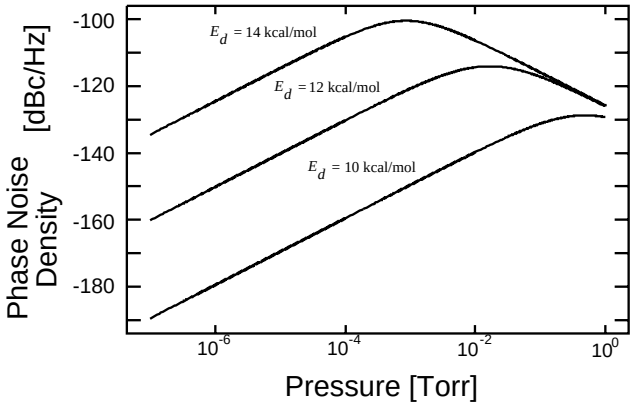

Fig. 11: Plot of mass loading-derived phase noise density (at a 100 Hz deviation from the carrier) versus pressure for a 10 MHz clamped-clamped beam µmechanical resonator at a temperature of 300K for contaminant molecules with the molecular weight of nitrogen and varying values of desorption activation energy.

Short-term Frequency Stability.

Short-term frequency stability is of utmost importance for oscillators used as carriers or local oscillators in communications and radar systems. Short-term stability is typically measured in terms of close to carrier phase noise power density, which is directly related to frequency noise power. Typical phase noise requirements range from –100 dBc/Hz at 270 kHz deviation from the carrier for the local oscillator in FDM/FM satellite communications networks [26] to –150 dBc/Hz at 67 kHz carrier deviations in Doppler-based radar systems [27].

Many phenomena contribute to phase noise in oscillators. The most commonly recognized phenomenon is superposed electronic noise from the sustaining amplifier. In the micromechanical domain, however, noise due to Brownian motion and mass loading have increased influence and may actually dominate among mechanisms that cause phase noise.

Superposed Electronic Noise.

The phase noise power due to superposed electronic noise from the sustaining amplifier may be predicted theoretically using a procedure similar to that in [26]. Assuming a linear series resonant oscillator, and thus, neglecting 1/*f* mixed noise, the equation for the relative oscillator phase noise power density N_{op} to carrier C power ratio at a deviation f_m from carrier frequency f_o is found to be [19]

$$\frac{N_{op}}{C} = \frac{FkT}{C}\frac{1}{8Q^2}\frac{R^2R_L}{(R_L+R_{in})^2R_{in}}\left(\frac{f_o}{f_m}\right)^2 \qquad (12)$$

where F is the amplifier noise figure, Q is the loaded quality factor of the resonator, R is the gain of the transresistance sustaining amplifier, R_{in} is the input resistance of the sustaining amplifier (Fig. 8), and R_L is the combination of the amplifier output resistance and the series motional resistance R_x of the µresonator.

Mass Loading Noise.

In addition to superposed electronic noise, any physical phenomenon that causes instantaneous frequency deviations of the resonator will contribute to the total phase noise power. Given that the typical mass of a µmechanical resonator is on the order of 10^{-11} kg, mass loading noise is expected to make a sizable contribution. Mass loading noise [6] arises from instantaneous differences in the rates of adsorption and desorption of contaminant molecules to and from the resonator surface, which cause mass fluctuations, and consequently, frequency fluctuations. Some of the factors which determine the magnitude of mass loading noise include the adsorption/desorption rate of contaminant molecules, contaminant molecule size and weight, pressure, and temperature.

An expression which estimates the phase noise density due to mass loading noise can be derived through a statistical analysis similar to that in [6]. Such analysis for the case of the flexural-mode capacitively transduced µresonators of this work yields for phase noise density [19]:

$$S_\phi(f) = \frac{s_o r_0 (\Delta f)^2/N}{(s_o r_0 + r_1)^2 + 4\pi^2 f^2}\cdot\frac{1}{f^2}, \qquad (13)$$

where f is the frequency deviation from the carrier at which phase noise is being calculated, r_o is the mean rate of arrival of contaminant molecules at a resonator site, s_o is the probability that the contaminant will stick to an uncontaminated site, r_1 is the desorption rate of molecules from the surface, and N is the total number of sites on the resonator surface at which adsorption or desorption can occur. Equation (13) assumes a sticking probability of zero if an adsorption site is contaminated, so the magnitude of phase noise predicted will be higher or lower than the actual value, depending upon the actual sticking probabilities for the molecules involved. The qualitative trends predicted by (13), however, are useful.

Pressure Dependence.

Using (13) and accounting for the pressure dependence of r_o [6], the phase noise density due to mass loading for a 10 MHz clamped-clamped beam µresonator can be plotted as a function of pressure. Figure 11 presents such a plot for phase noise density versus pressure at a 100 Hz deviation from the carrier, where a

contaminant molecule with the molecular weight of nitrogen has been assumed, at a constant temperature of 300 K and for varying values of desorption activation energy. In this curve, a strong dependence on the contaminant desorption activation energy is seen. In addition, for each of the curves, the mass loading phase noise density is largest at an intermediate value of pressure and smallest at the higher and lower pressures. This is reasonable when one considers that at high pressures, the resonator may be saturated with contaminant molecules and little transfer to and from the surface occurs. At extremely low pressures, very few contaminants are present, and the flux of contaminant molecules is likewise small. It is at intermediate pressures where transfer of contaminant molecules is maximized, and consequently, mass loading-derived phase noise peaks.

As previously mentioned, μmechanical resonators exhibit high-*Q* when operated under low pressures, in the range of 0.1 to 1 mTorr. However, these pressures may still not be low enough to achieve high-*Q* resonators with minimum phase noise. As seen from Fig. 11, the phase noise density due to mass loading may still be large at these pressures, and even lower pressures may be required to alleviate this noise source. Thus, given a required phase noise density level, mass loading may set an upper limit on operation pressure, and in this way, may ultimately dictate the design of the most stable μmechanical resonator oscillators.

On-chip vacuum encapsulation techniques have been previously investigated which provide vacuums with pressures below 100 mTorr [30], or perhaps better [31]. Encapsulation strategies which use gettering elements to remove residual gases may potentially provide the even lower pressure ranges (10^{-7} to 10^{-6} Torr) requested by Fig. 11.

Temperature Dependence.

In addition to a dependence upon pressure, mass loading noise depends upon temperature as well. This dependence arises mainly from the temperature dependence of the rates of adsorption and desorption of contaminants [6]. Using Eq. (13), the mass loading-derived phase noise density for the 10 MHz parallel-plate clamped-clamped beam resonator of Fig. 11 at 100 Hz frequency deviation from the carrier and for the pressure where mass loading noise peaks (1 mTorr), is shown as a function of temperature in Fig. 12 . As seen in the plot, the effect of mass loading on the short term frequency stability of a resonator should taper off as temperatures increase. This suggests that a low power micro-oven, such as described in [2], could be used to substantially reduce phase noise contributions due to mass loading.

MICROELECTROMECHANICAL FILTERS

Simple second-order high-*Q* bandpass filters are often required in communication electronics. A single μmechanical resonator can provide a high-*Q* bandpass or lowpass biquad response, depending upon whether resistive or capacitive detection techniques are utilized [19]. A typical measured response for an 18 kHz folded-beam comb-driven μmechanical resonator operated under 20 mTorr pressure was presented in Fig. 5, which indicated a quality factor of 50,000 and an effective 3 dB-down bandwidth of 0.36 Hz.

For most practical applications, however, filter responses with larger bandwidths, flatter passbands, higher stopband rejection, and steeper passband-to-stopband transitions are required. To

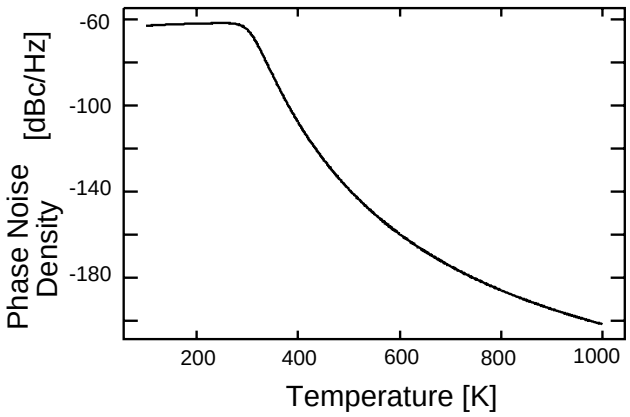

Fig. 12: Plot of phase noise density caused by mass loading versus temperature for 10 MHz parallel-plate clamped-clamped beam resonator at 100 Hz frequency deviation from the carrier and for the pressure where mass loading noise peaks (1 mTorr).

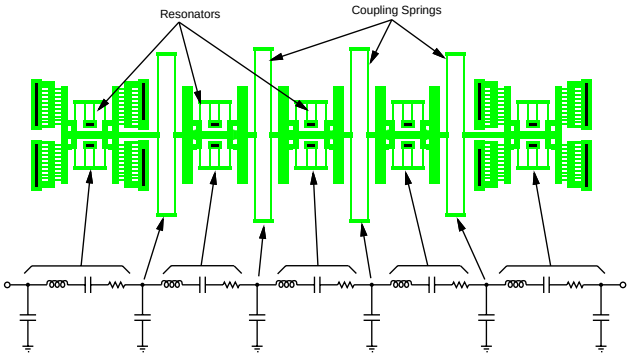

Fig. 13: Schematic of a five-resonator μmechanical filter, explicitly showing electromechanical equivalencies.

achieve such characteristics, higher order filters are needed, generally consisting of a network of tank elements coupled via energy storage elements. In the micromechanical domain, this network of elements may be achieved by coupling mechanical resonators via soft mechanical springs.

Figure 13 presents the schematic of a five-resonator micromechanical filter. As explicitly shown in the figure, such filters are designed through use of electromechanical analogies, where the electrical domain inductance and capacitance of a properly synthesized LC ladder filter are implemented via analogous values of compliance and mass in the mechanical domain. As previously discussed, resonators in the mechanical domain equate to LCR tanks in the electrical domain, while coupling springs are analogous to coupling shunt capacitors. Mechanical filters can thus be designed by first synthesizing an LC ladder filter to satisfy required specifications, then designing a mechanical network similar to that of Fig. 13, with values of mass, compliance, and transducer coupling coefficient chosen such that the electrical and mechanical circuits are equivalent.

In order to realize a specific filter bandwidth, the quality factor *Q* of the constituent resonators must be controlled to some degree. As is demonstrated later, for the case of two-resonator mechanical filters, such *Q*-control can be achieved via control of the ambient pressure. However, for the general case of high order

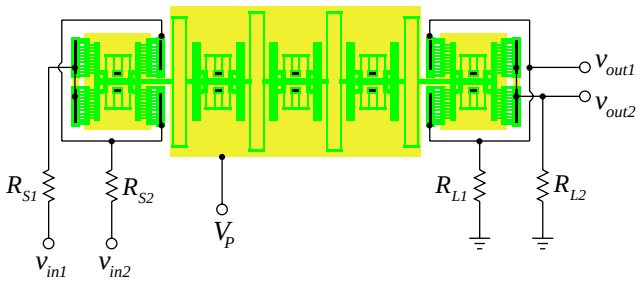

Fig. 14: Schematic showing the resistive terminations required for bandwidth control of a balanced μmechanical filter.

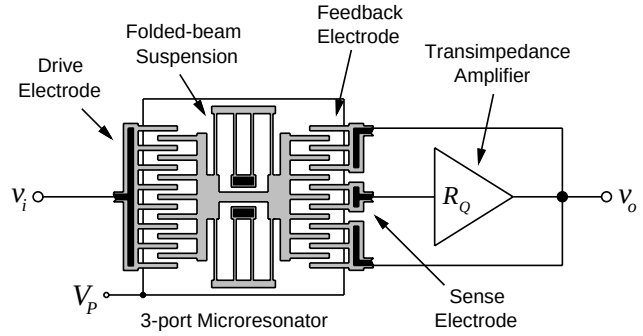

Fig. 15: Circuit schematic for active Q-control of a three-port μresonator.

filters, more selective Q-control is required, in which each constituent resonator may require a unique value of Q. For example, in many designs the Q of the end resonators must be reduced, but the Q of the internal resonators must remain large.

The simplest method for controlling the Q of end resonators is to use terminating resistors in series with the filter input and output, as shown in Fig. 14. In this figure, a balanced excitation and detection scheme, in which a differential input is applied, is shown. Balanced operation is advantageous for two reasons: first, the effective electromechanical coupling is increased since a larger number of fingers can be used; second, highly linear balanced detection circuitry can be utilized. The value of terminating resistance R_s required for a given filter is proportional to the size of the motional resistance R_x of its end resonators, given by Eq. (6). For present-day micromachining technologies, and for reasonable values of dc-bias voltage, R_x is on the order of hundreds of kilo-ohms, and corresponding values of R_s are in the range of tens of megaohms—impractically large for most IC processes, and large enough to contribute substantial dynamic range degradation.

Thus, an alternative method for controlling μresonator Q is required. Since the initial quality factor of the μmechanical resonator is difficult to predict, any technique used to control Q should be independent of its initial value. One Q-control method which satisfies the above condition and provides ratioed specification of the effective gain of the stage is shown in Fig. 15. Here, a three-port μmechanical resonator is utilized, where an input port accepts an excitation signal, an output port directs resonator motional current to a transresistance amplifier, and a feedback port directs the resulting output voltage back to the resonator. Properly phased competition between the input and feedback

Fig. 16: Experimental demonstration of Q-control. Each μresonator transfer function corresponds to a different value of Q-controlling (trans)resistance R_Q. The measured values of Q are 53,000 for R_Q=1MΩ and 17,000 for R_Q=3.3MΩ.

ports effectively lowers the Q of the system. Using the equivalent circuit for a multi-port μresonator [1,19], the transfer function for the system of Fig. 15 can be written as:

$$\frac{v_o}{v_i}(j\omega) = \frac{N_i}{N_{fb}} \frac{1}{1 + 2jQ'(\Delta\omega/\omega_o)}, \tag{14}$$

where

$$Q' = \frac{[M_{eff} k_{sys}]^{\frac{1}{2}}}{V_P^2 \left(\frac{\partial C}{\partial x}\right)_{fb} \left(\frac{\partial C}{\partial x}\right)_o R_Q} \tag{15}$$

is the controlled value of quality factor when the initial unloaded resonator Q is large. In Eq. (14), M_{eff} and k_{sys} are the effective mass and spring constant of the resonator, respectively, N_i is the number of resonator input fingers, N_{fb} is the number of resonator feedback fingers, and R_Q is the transresistance amplification provided by the amplifier. Note that from (15), Q' is independent of the original quality factor Q of the resonator. Note that the gain of this stage is completely determined by the ratio of the number of resonator input fingers N_i to the number of feedback fingers N_{fb} which can be precisely specified to within an error dependent upon the matching tolerance of the $\partial C/\partial x$ for each finger gap. This, combined with Q variability, provides complete freedom in specifying almost any arbitrary bandpass biquad transfer function via this μelectromechanical system.

Using a fabricated multi-port resonator and off-chip electronics, control of Q via this technique is demonstrated in Fig. 16, which shows a plot of the resonator transconductance spectrum under varying values of Q-controlling transimpedance, R_Q.

Utilizing this active Q-control technique, the schematic diagram for a passband-controllable μmechanical filter is presented in Fig. 17.

Dynamic Range of Microelectromechanical Filters.

The dynamic range of integrated electronic filters is generally limited by electronic noise. For the case of micromechanical filters, Brownian motion noise can play a dominant role in setting

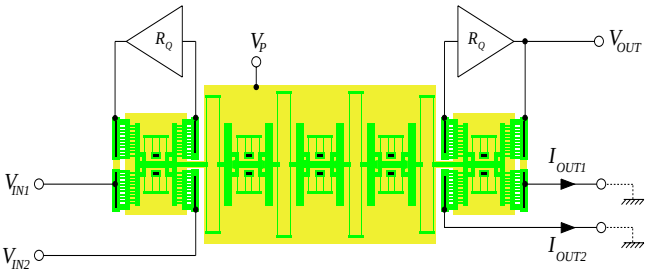

Fig. 17: Schematic for a μmechanical filter utilizing active *Q*-control to control the passband shape and bandwidth. (Note that this is a schematic drawing intended for clarity. The actual placement of electrodes is more symmetrical than indicated here.)

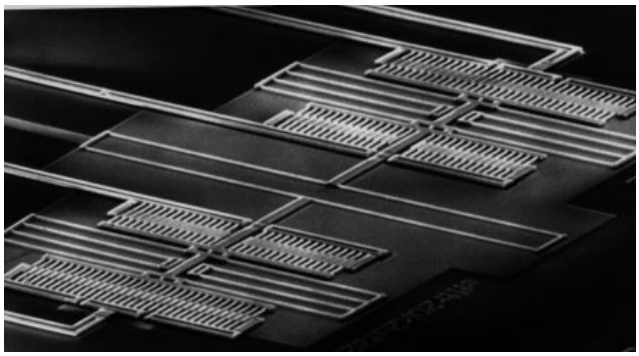

Fig. 18: SEM of a two-resonator spring-coupled μmechanical filter.

the dynamic range in the absence of defensive design strategies that minimize this noise source.

In this respect, the choice of the *Q*-controlling scheme for a given μmechanical filter can have a significant effect on the total dynamic range. This is because he magnitude of the input-referred noise for a given filter is strongly dependent on the *Q*-control scheme used. To see this, first consider the resistively terminated filter shown in Fig. 14. Applying standard noise analysis [28], the equivalent input-referred voltage noise source in the passband of this filter is found to be [19]

$$\overline{v_i^2} = \overline{v_{R_s}^2} + \overline{v_{R_{xs}}^2} + \overline{v_{ia}^2} + \overline{i_{ia}^2} R_{xs}^2 , \tag{16}$$

where $\overline{v_{R_s}^2}$ represents voltage noise due to the effective termination resistance R_s, $\overline{v_{R_{xs}}^2}$ represents voltage noise due to the total series resistance through the filter, and $\overline{v_{ia}^2}$ and $\overline{i_{ia}^2}$ are the input-referred noise sources associated with an amplifier connected to the output electrode [19,28]. The voltage noise generator associated with a resistor with value R is given by [28]

$$\overline{v_R^2} = 4k_B T R \Delta f , \tag{17}$$

where Δf is the bandwidth of interest. Note that from (17) the input referred voltage noise source $\overline{v_i^2}$ is a function of R_s, which is usually much larger than R_x, and which thus, dominates the total voltage noise.

For the active *Q*-control technique of Fig. 15, the equivalent input-referred passband voltage noise source is found to be

$$\overline{v_i^2} = \overline{v_{R_x}^2} + \overline{v_{ia}^2}\left(\frac{R_{xi\cdot o}}{R_{xo}}\right)^2 + \overline{i_{ia}^2} R_{xi\cdot o}^2 , \tag{18}$$

where $R_{xi\cdot o}$ is the effective motional resistance seen between the input and output transducers in Fig. 15, and R_{xo} is the resistance looking into the output transducer [1,19]. Note that the input-referred voltage noise source is no longer dependent upon the *Q*-controlling transresistance, and thus, depending upon the magnitude of $\overline{v_{ia}^2}$ and $\overline{i_{ia}^2}$, can be many times smaller than for the case of Fig. 14. In addition to noise advantages, the active *Q*-controlling technique can achieve higher operation frequency, as well [19].

Of the noise sources comprising $\overline{v_i^2}$ in Eq. (18), $\overline{v_{R_x}^2}$ (which represents Brownian motion noise) will dominate, since R_x is large. Thus, Brownian noise as modelled by R_x can play an important role in limiting the dynamic range of a given μmechanical filter. For example, a resonator with R_x=300kΩ would contribute a voltage noise generator in the range of 70.6 nV/$\sqrt{\text{Hz}}$, which results in a dynamic range of 100 dB for a maximum voltage swing of 3V. To achieve a higher dynamic range the value of R_x must be lowered. Equation (6) suggests that this can be achieved by reducing the mass m and stiffness k of the resonator, and by increasing the value of the electromechanical coupling factor η. An increase in η can be achieved by increasing both the dc-bias V_P and the value of $\partial C/\partial x$. Since the dc-bias V_P is limited by the power supply of the chip, increases in η will come mainly from increases in $\partial C/\partial x$. Equations (3) and (5) suggest that for the case of a capacitively transduced resonator, $\partial C/\partial x$ may be increased by decreasing the capacitive gap spacings from resonator to electrode. Thus, technologies that can achieve fine gaps between conductors will play a central role in the realization of high dynamic range, fully integrated, high-*Q* filters.

A Fabricated Two-Resonator Filter.

The SEM for a fabricated polycrystalline silicon spring-coupled micromechanical filter is presented in Fig. 18. As shown, multiport μresonators were utilized in the filter to enable active *Q*-control of the resonators. However, due to large off-chip parasitics (that would not be present if integrated circuitry were available), the limited bandwidths of off-chip components did not allow sufficient *Q*-control. To circumvent this problem, the *Q* of the μresonators was instead controlled by carefully controlling the ambient operation pressure, taking advantage of the susceptibility of micromechanical resonators to viscous gas damping. This was done using an MMR vacuum probe station, which allows control of the pressure in a small evacuated chamber via the admission of controlled amounts of nitrogen. Using this system, the operating pressure (and thus, the resonator *Q*) was tweaked to yield a relatively flat filter passband. The measured spectrum for the fabricated two-resonator filter is shown in Fig. 19.

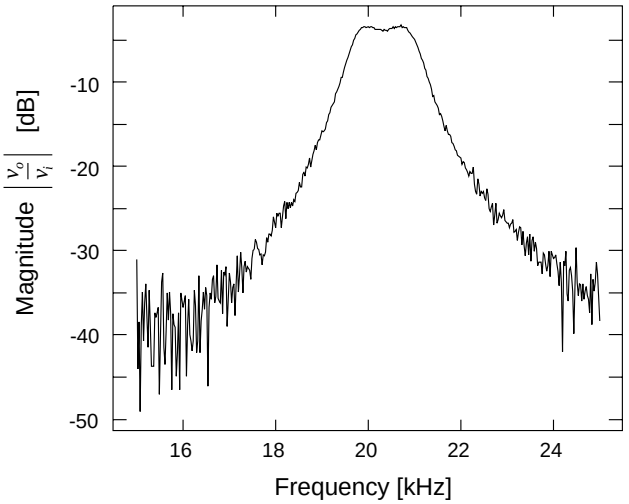

Fig. 19: Measured transfer function for the two-resonator μmechanical filter of Fig. 18.

THERMAL STABILIZATION VIA A MICRO-OVEN

As measured (Fig. 6), the temperature coefficient of the resonance frequency TC_{fr} for a uniformly n+ doped polycrystalline silicon, folded-beam, comb-driven μmechanical resonator is on the order of -10 ppm/°C in a temperature range from 300K to 370K. This is higher than AT-cut quartz, which has uncompensated temperature coefficients from -2 to 2 ppm/°C for temperatures ranging from 200K to 370K [33].

To improve the TC_{fr} for μmechanical resonators, temperature compensation or oven control techniques may be implemented. For the case of quartz crystals, oven control has generally yielded the greatest reductions in TC_{fr} [33]. Despite this, oven controlled crystal oscillators are much less used than their temperature compensated counterparts, because they often require large volumes, warm-up times from 2 to 30 minutes, and substantial amounts of power (1 to 10 Watts) [33].

On the micro-scale, however, these drawbacks can be greatly alleviated. Figure 20 presents the SEM of an integrated micro-oven, supporting a μmechanical resonator. The micro-oven consists of a nitride platform suspended 2 μm above the silicon substrate via long, thin, folded struts. The suspending struts, which can be polysilicon or a poly/nitride sandwich, provide thermal isolation of the platform from the substrate, as well as conductive interconnect between these media. These struts are folded to relieve post-fabrication stress, preventing possible buckling of the platform. In addition to providing stress relief, folding also increases the effective length of the struts, increasing the conductive thermal resistance from the platform to the substrate. Heating and sensing resistors are also fabricated on the platform for use in temperature-setting feedback circuitry. Due to the high degree of thermal isolation afforded by the platform suspension, very little power is required to maintain high temperature. As seen in the plot, only 22 mW is required to maintain 1000K, while only 2 mW achieves 370K [2]. Furthermore, due to the tiny volumes involved, thermal time constants are on the order of milliseconds.

By embedding the on-platform heater and temperature sens-

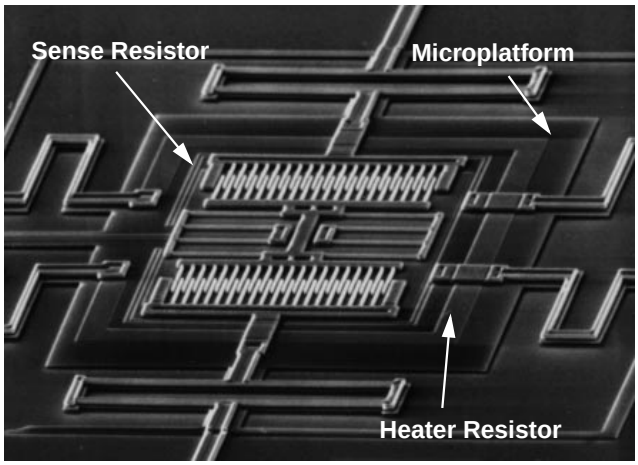

Fig. 20: SEM of an integrated micro-oven, comprised of a thermally isolated μplatform with on-platform heating and temperature sensing resistors, and a polysilicon μmechanical resonator.

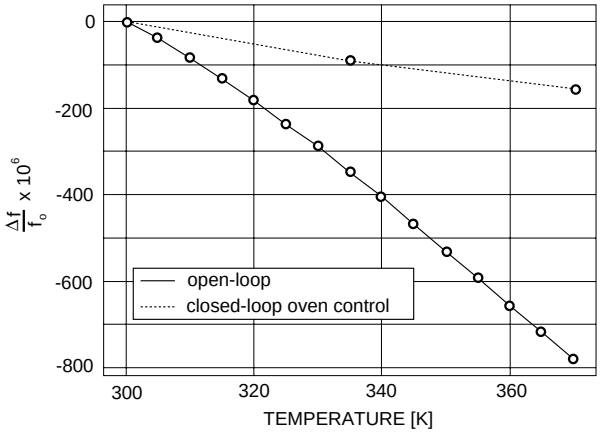

Fig. 21: Plot of ppm change in resonance frequency vs. temperature for a polysilicon μmechanical resonator on a thermally insulating platform, comparing resonator thermal performance with and without closed loop oven control.

perature of the on-platform polysilicon μmechanical resonator can be stabilized with respect to its surroundings. Figure 21 shows a comparison of the fractional frequency vs. temperature curves for the on-platform μresonator with and without temperature-setting feedback circuitry. With oven control, the TC_{fr} is 2 ppm/°C—a 5 times reduction of the previous uncontrolled value.

CONCLUSIONS

Fully monolithic, highly stable, high-*Q* oscillators and electromechanical filters utilizing surface-micromachined polysilicon mechanical resonators have been demonstrated. Due to the novelty of the process and the devices, conservative measures were taken for the designs, and prototypes of up to only 100 kHz were fabricated. Designs up to a few megaHertz are feasible using folded-beam resonator designs, and higher frequencies (tens of MHz) should be feasible using more advanced designs aimed at maximizing resonator quality factor, which may otherwise degrade with increasing frequency. Both material and architec-

tural improvements should increase μresonator *Q*. In addition, as frequency increases, smaller electrode-to-resonator gaps will be required to minimize Brownian noise and maintain reasonable (low) values of series motional resistance.

The basic issues associated with miniaturization of high-*Q* elements were addressed via analysis and experimental verification of these systems. Brownian motion and mass loading were identified as phenomena which become increasingly important contributors to phase noise as resonator dimensions shrink. Brownian noise may also greatly influence the dynamic range of micromechanical filters if strategies that reduce its effects are not implemented. Brownian noise may be reduced by decreasing the electrode-to-resonator gap spacings, or through other strategies that maximize electromechanical transducer coupling. According to theory, mass loading-induced phase noise can be substantially reduced by operating the miniature μmechanical resonator under optimum pressure and temperature. For this reason, integrated vacuum encapsulation and micro-oven techniques may play central roles in achieving minimum phase noise.

ACKNOWLEDGEMENT

The author would like to thank Prof. Roger T. Howe from the University of California at Berkeley for insightful contributions to the oscillator work. In addition, I am grateful for discussions with John Vig of the U.S. Army Electronics Technology and Devices Laboratory, whose insights on mass loading contributed much to this work.

REFERENCES

[1] C. T.-C. Nguyen and R. T. Howe, "Quality factor control for micromechanical resonators," *Technical Digest*, IEEE International Electron Devices Meeting, San Francisco, California, December 14-16, 1992, pp. 505-508

[2] C. T.-C. Nguyen and R. T. Howe, "Microresonator frequency control and stabilization using an integrated micro oven," *Digest of Technical Papers*, the 7th International Conference on Solid-State Sensors and Actuators (Transducers'93), Yokohama, Japan, pp. 1040-1043, June 7-10, 1993.

[3] C. T.-C. Nguyen and R. T. Howe, "CMOS Micromechanical Resonator Oscillator," *Technical Digest*, IEEE International Electron Devices Meeting, Washington, D. C., pp. 199-202, December 5-8, 1993.

[4] C. T.-C. Nguyen and R. T. Howe, "Design and performance of monolithic CMOS micromechanical resonator oscillators," *Proceedings*, 1994 IEEE International Frequency Control Symposium, Boston, MA, May 31-June 3, 1994, pp. 127-134.

[5] C. T.-C. Nguyen and R. T. Howe, "Polysilicon microresonators for signal processing," *Digest of Papers*, Government Microcircuit and Applications Conference, San Diego, CA, Aug. 15, 1994, pp. 195-198.

[6] Y. K. Yong and J. R. Vig, "Resonator surface contamination—a cause of frequency fluctuations?" *IEEE Trans. Utrason. Ferroelec. Freq. Contr.*, vol. 36, no. 4, pp. 452-458, March 1989.

[7] R. T. Howe and R. S. Muller, "Resonant microbridge vapor sensor," *IEEE Trans. Electron Devices*, ED-33, pp. 499-506, 1986.

[8] H. Nathanson, W. E. Newell, R. A. Wickstrom, and J. R. Davis, Jr., "The resonant gate transistor," *IEEE Trans. Electron Devices*, vol. ED-14, No. 3, pp. 117-133, March 1967.

[9] L. Meirovitch, *Analytical Methods in Vibrations*. New York: Macmillan Publishing Co., Inc., 1967.

[10] W. C. Tang, T.-C. H. Nguyen, and R. T. Howe, "Laterally driven polysilicon resonant microstructures," *Sensors and Actuators*, **20**, 25-32, 1989.

[11] W. C. Tang, "Electrostatic Comb Drive for Resonant Sensor and Actuator Applications," Ph.D. Dissertation, Dept. of Electrical Engineering and Computer Sciences, University of California, Berkeley CA, Sept. 1989.

[12] G. K. Fedder, "Simulation of Microelectromechanical Systems," Ph.D. Dissertation, Dept. of Electrical Engineering and Computer Sciences, University of California at Berkeley, September 1994.

[13] M. W. Judy, "Micromechanisms Using Sidewall Beams," Ph.D. Dissertation, Dept. of Electrical Engineering and Computer Sciences, University of California at Berkeley, April 1994.

[14] M. Christen, "Air and gas damping of quartz tuning forks," *Sensors and Actuators*, 4 (1983), pp. 555-564.

[15] R. A. Buser, "Theoretical and experimental investigations of silicon single crystal resonant structures," Ph.D. Thesis, Inst. of Microtechnology, University of Neuchatel, CH-2000 Neuchatel, Switzerland, July 1989.

[16] Y.-H. Cho, A. P. Pisano, and R. T. Howe, "Viscous damping model for laterally oscillating microstructures," *J. Microelectromech. Syst.*, vol. 3, no. 2, pp. 81-87, June 1994.

[17] T. V. Rozhart, "The effect of thermoelastic internal friction on the Q of micromachined silicon resonators," *Technical Digest* of the IEEE Solid-State Sensor and Actuator Workshop, Hilton Head, South Carolina, pp. 13-16, June 4-7, 1990.

[18] V. B. Braginskky, V. P. Mitrofanov, and V. I. Panov, *Systems With Small Dissipation*. Chicago: University of Chicago Press., 1985.

[19] C. T.-C. Nguyen, "Micromechanical Signal Processors," Ph.D. Dissertation, Dept. of Electrical Engineering and Computer Sciences, University of California at Berkeley, December 1994.

[20] L. Lin, C. T.-C. Nguyen, R. T. Howe, and A. P. Pisano, "Micro electromechanical filters for signal processing," *Technical Digest*, IEEE Micro Electromechanical Systems Workshop, Travemunde, Germany, pp. 226-231, Feb. 4-7, 1992.

[21] H. Guckel, *et al.*, "The mechanical properties of fine-grained polysilicon: the repeatability issue," Technical Digest, IEEE Solid-State Sensor and Actuator Workshop, Hilton Head Island, S. C., June 1988, pp. 96-99.

[22] F. S. Crawford, "Elementary derivation of the law of equipartition of energy," Am J. Phys., 55, pp. 180-182 (1987).

[23] T. B. Gabrielson, "Fundamental noise limits in miniature acoustic and vibration sensors," Phase Report, Report No.NADC-91113-50, Dec. 31, 1991.

[24] B. E. Boser and R. T. Howe, "Surface micromachined accelerometers," *Proceedings*, the 17th Annual Custom Integrated Circuits Conference, Santa Clara, CA, pp. 337-344, 1995.

[25] E. A. Gerber, A. Ballato, Editors, *Precision Frequency Control, Volume 2: Oscillators and Standards*. New York: Academic Press, Inc., 1985.

[26] W. P. Robins, *Phase Noise in Signal Sources*. London: Peter Peregrinus, Ltd., 1982.

[27] N. Slawsby, "Frequency control requirements of radar," *Proceedings* of the 1994 IEEE International Frequency Control Symposium, June 1-3, 1994, pp. 633-640.

[28] P. R. Gray and R. G. Meyer, *Analysis and Design of Analog Integrated Circuits*, 2nd Ed. New York: John Wiley & Sons, 1984.

[29] M. Prutton, *Surface Physics, 2nd ed*. Oxford: Clarendon Press, 1983.

[30] L. Lin, *et al*, "Vacuum-encapsulated lateral microresonators," *Technical Digest*, 7th International Conference on Solid-State Sensors and Actuators (Transducers'93), Yokohama, Japan, June 1993, pp. 270-273.

[31] H. Guckel, *et al*, "Polysilicon resonant microbeam technology for high performance sensor applications," *Technical Digest*, IEEE Solid-State Sensor & Actuator Workshop, Hilton Head Island, South Carolina, June 22-25, 1992., pp. 153-156.

[32] W. Yun, R. T. Howe, and P. R. Gray, "Surface micromachined, digitally force-balanced accelerometer with integrated CMOS detection circuitry, *Technical Digest*, IEEE Solid-State Sensor & Actuator Workshop, Hilton Head Island, South Carolina, June 22-25, 1992, pp. 126-131.

[33] M. E. Frerking, *Crystal Oscillator Design and Temperature Compensation*. New York: Van Nostrand Reinhold, 1978.